Structure, Vol. 12, 611–622, April, 2004, ©2004 Elsevier Science Ltd. All rights reserved. DOI 10.1016/j.str.2004.02.019

Solution Structure of ZASP PDZ Domain: Implications for Sarcomere Ultrastructure and Enigma Family Redundancy

Yunghan Au,[1] R. Andrew Atkinson,[2] Remo Guerrini,[3] Geoff Kelly,[1] Catherine Joseph,[1] Steven R. Martin,[1] Frederick W. Muskett,[1] Alberto Pallavicini,[4] Georgine Faulkner,[5] and Annalisa Pastore[1,*]

[1]National Institute for Medical Research
The Ridgeway
Mill Hill
London, NW7 1AA
United Kingdom

[2]Laboratoire de Biologie et de Génomique Structurales
Groupe de RMN
UMR 7104 CNRS, ESBS, bd Sébastien Brant, BP 10413
67412 Illkirch Cedex
France

[3]Department of Pharmaceutical Sciences and Biotechnology Centre
University of Ferrara
via Fossato di Mortara, 17/19
44100 Ferrara

[4]Department of Biology
University of Trieste
34127 Trieste

[5]International Centre for Genetic Engineering and Biotechnology
34012 Trieste
Italy

Summary

Z band alternately spliced PDZ-containing protein (ZASP) is a sarcomere Z disk protein expressed in human cardiac and skeletal muscle that is thought to be involved in a dominant familial dilated cardiomyopathy. The N-terminal PDZ domain of ZASP interacts with the C terminus of α-actinin-2, the major component of the Z disk, probably by forming a ternary complex with titin Z repeats. We have determined the structure of ZASP PDZ by NMR and showed that it is a classical class 1 PDZ domain that recognizes the carboxy-terminal sequence of an α-actinin-2 calmodulin-like domain with micromolar affinity. We also characterized the role of each component in the ternary complex ZASP/α-actinin-2/titin, showing that the α-actinin-2/ZASP PDZ interaction involves a binding surface distinct from that recognized by the titin Z repeats. ZASP PDZ structure was used to model other members of the enigma family by homology and to predict their abilities to bind α-actinin-2.

Introduction

The sarcomere is a network of filamentous proteins and membranes that form the basic repeating unit of muscles that is necessary for muscle contraction (Figure 1). An essential component is the multiprotein complex known as the Z disk, which seems to have multiple functions that range from keeping the microscopic structure of the sarcomere in register, to transmitting the tension during contraction while serving a myocyte cell signaling role (Clark et al., 2002). The major component of the Z disk is the muscle-specific α-actinin-2 isoform, a multidomain protein that tethers major proteins such as actin and titin within the sarcomere (Faulkner et al., 2001).

α-actinin-2 is involved in a complex network of interactions. Among its many partners is ZASP, a relatively small protein found only in the Z disk of skeletal and cardiac muscles (Faulkner et al., 1999). ZASP belongs to the enigma family of cytoskeletal proteins, with which it shares a similar architecture. Although no definite role has yet been established, cypher (the murine ZASP ortholog) knockout mice display a severe form of congenital myopathy and die from functional failure in multiple striated muscles (Zhou et al., 2001), thus suggesting that ZASP is required for maintaining the cytoskeletal ultrastructure during contraction. In humans, ZASP is thought, together with other Z disk proteins, to be involved in the autosomal dominant form of familial dilated cardiomyopathy (DCM) (Bowles et al., 2000; Gerull et al., 2002; Knoll et al., 2002), a primary cardiac muscle disease characterized by left ventricular dilatation and systolic dysfunction (Goodwin, 1982; Johnson and Palacios, 1982; Sugrue et al., 1992).

The interaction between ZASP and α-actinin-2 has been mapped to the ZASP PDZ domain and to the C terminus of α-actinin-2 (Faulkner et al., 1999; Zhou et al., 2001). PDZs are protein modules of 80–120 residues involved in targeting and clustering of membrane proteins or directing cellular proteins to multiprotein complexes (for a review see Hung and Sheng, 2002). Three types of interaction involving PDZ motifs have been described in detail (Hung and Sheng, 2002). The first two types, class 1 and 2, involve binding of carboxy-terminal protein sequences through either a -(S/T)-x-(V/I/L) or a -(F/Y)-x-(F/V/A) sequence motif. The third type of recognition involves internal -(S/T)-x-V- sequence motifs. The C terminus of α-actinin-2 contains a calmodulin-like domain with four EF-hand motifs that have lost their calcium binding properties (Beggs et al., 1992). EF-hands 3 and 4 are also involved in the interaction with the Z repeats of titin (Sorimachi et al., 1997; Young et al., 1998).

Despite the structural role that the α-actinin-2/ZASP interaction may play in the sarcomere, no description of the interaction at atomic resolution is currently available. An important question is whether or not α-actinin-2/ZASP recognition competes with other α-actinin-2 interactions, such as those with titin Z repeats, thus requiring a major rearrangement of the α-actinin-2 structure to accommodate multiple complexes. It is also interesting to understand if and how other members of the enigma family could compete the α-actinin-2 interac-

*Correspondence: pastoreteam@nimr.mrc.ac.uk

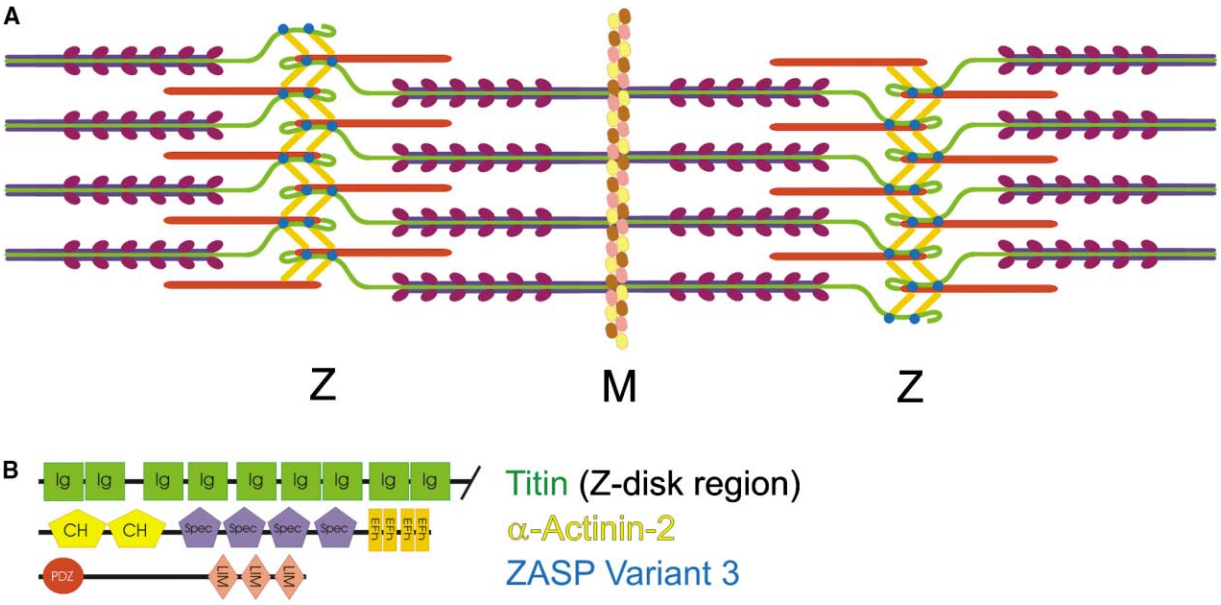

Figure 1. Diagram of the Sarcomere and Domain Architecture

(A) Schematic representation of the sarcomere. The position of the Z disk and of the M line is indicated. A single molecule titin filament (indicated in green) connects the Z disk to the M line. In the Z disk, α-actinin-2 (in yellow) forms transversal connections between actin filaments (in red) and is thought to bind ZASP (in blue).

(B) Domain architecture of the titin region localized in the Z disk, α-actinin-2, and ZASP (variant 3).

tion. To address these questions, we solved the structure of a construct spanning the sequence of ZASP PDZ (ZASP-PDZ) and studied its interaction with α-actinin-2 using nuclear magnetic resonance (NMR) spectroscopy supported by fluorescence studies. Our results are consistent with ZASP PDZ being a classical class 1 PDZ domain which recognizes the carboxy-terminal sequence of an α-actinin-2 calmodulin-like domain with micromolar affinity. We explored the possibility of the mutual coexistence of an α-actinin-2/ZASP complex with titin/α-actinin-2 interactions by characterizing both a binary and a ternary complex. We observed that the α-actinin-2/ZASP PDZ interaction involves a binding surface distinct from that recognized by the titin Z repeats, thus supporting the possibility of a ternary complex. Finally, we used the ZASP-PDZ coordinates as a template for building homology models of other PDZ domains from the enigma family and to map conserved residues that could be functionally important. Based on the pattern of conservation, we make testable predictions about which members of the family are likely to have α-actinin-2 binding properties.

Results

Structure Calculations

The ZASP-PDZ sample gave rise to excellent NMR spectra (Figure 2). These led to a straightforward spectral assignment. For training purposes, two different strategies were used for structure calculation, based on a manual (MANUAL) and an automatic (CANDID) assignment of the NOESY information (see Experimental Procedures). Both bundles were further refined against the residual dipolar coupling (RDC) restraints (XMANUAL and XCANDID runs) and finally improved with a water refinement protocol (RXMANUAL and RXCANDID) (Spronk et al., 2002). Comparison of the manual and automatic assignment shows that although CANDID makes more intraresidue assignments (+6.6%) and fewer short-range assignments (−6.0%), there is not a significant difference between the distribution of medium (−1.2%) and long-range restraints (+0.62) (Table 1).

Precision and Accuracy of the Resulting ZASP-PDZ Structures

The resulting CANDID bundles are more compact than those from the MANUAL calculation with a lower rmsd with or without further refinement, implying a higher precision (Figure 3). To estimate the accuracy of our results, we compared them with the known structures of PDZ domains, as suggested in (Walma et al., 2002). A DALI structural similarity search (Holm and Sander, 1996b) identified six structures with rmsd values between 2.5 and 3.0 Å and sequence identities ranging between 21% and 30%, all corresponding to PDZ domains. The highest similarity is with the crystal structure of the third PDZ domain from human disks large protein (DlgA, entry code 1pdr [Morais Cabral et al., 1996]) which superposes ZASP-PDZ with an rmsd of 2.0 Å (Z score of 11.1, 23% sequence identity). Pairwise comparison of 1pdr with the high-resolution crystallographic structures of two representatives of the major interaction classes (CASK and syntrophin corresponding to 1kwa and 1qav respectively [Doyle et al., 1996; Hillier et al., 1999]) shows that the structural variability between our final bundles is in regions with the largest variability within different PDZ domains (Figure 4). This would suggest that the two bundles have a comparable accuracy.

On the other hand, the RDC restraints have a smaller effect on the CANDID run than on the manual calculation,

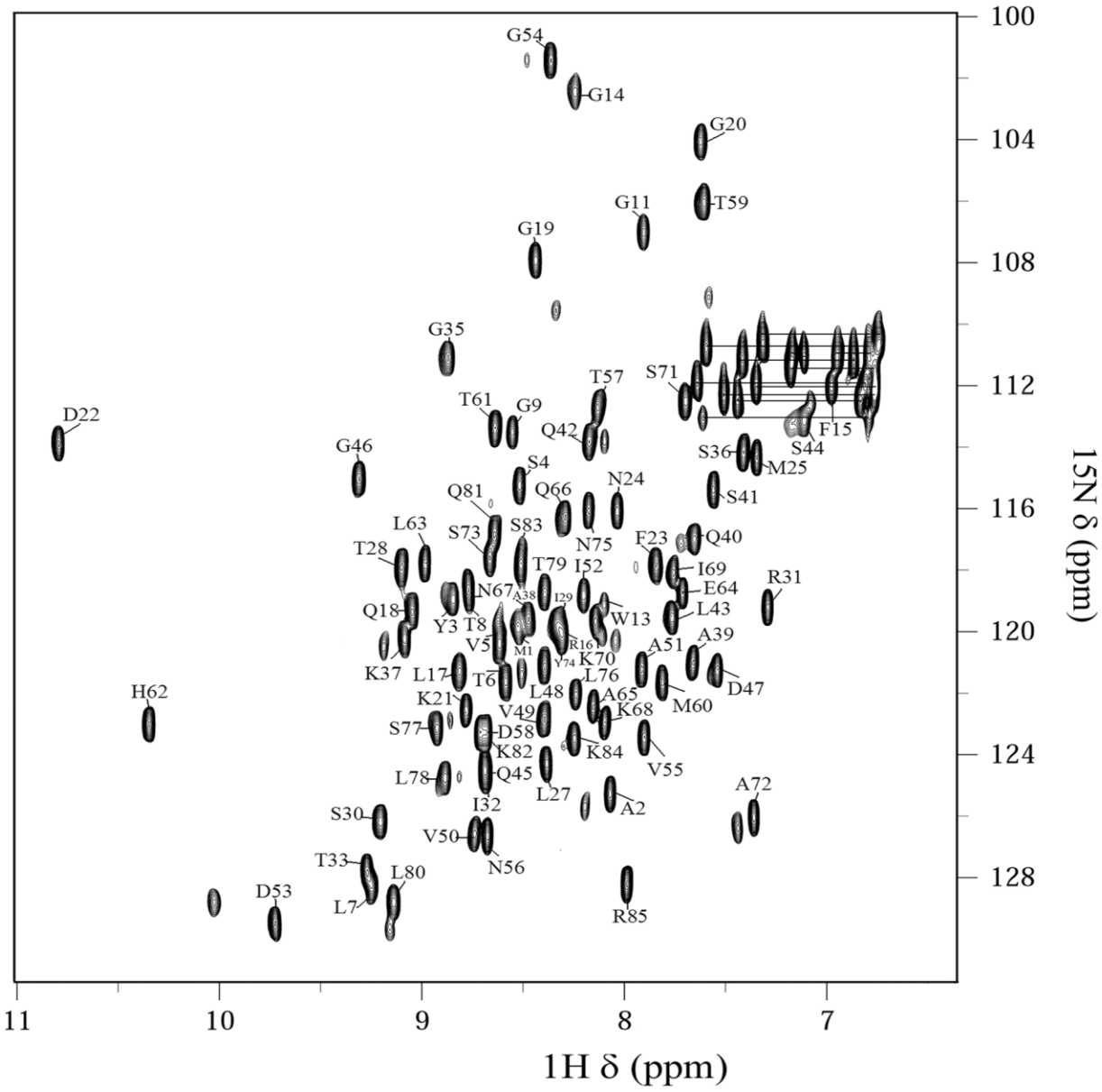

Figure 2. A 500 MHz ^{1}H-^{15}N HSQC Spectrum of ZASP-PDZ at pH 6.6 and 27°C Showing Backbone Resonance Assignments

Side chain amide protons of asparagine and glutamine residues are indicated by solid horizontal lines.

Table 1. Comparison of the Manual and Automatic Assignment of ZASP-PDZ

	CANDID	MANUAL
Restraints		
Intraresidue	265 (31.1%)	219 (24.5%)
Short range	227 (26.6%)	292 (32.6%)
Medium range	126 (14.8%)	143 (16.0%)
Long range	235 (27.5%)	241 (26.9%)
Angular restraints		
ϕ	51	51
ψ	46	46
H bonds	30	7
Total no. of restraints	980	998
RDCs[a]	63	63
Stereospecific assignments	25	25

[a] Only added to the XCANDID and XMANUAL refinements.

implying a better agreement with the automatically calculated NOE distance restraints. Consistently, the structure quality as assessed by WHATIF and PROCHECK-NMR is better for the CANDID run (Table 2). Since the automatic assignment procedure is not only faster (taking hours rather than weeks), but also more efficient and less subject to biased choices than the MANUAL procedure, we considered the RXCANDID bundle as representative of the structure of ZASP-PDZ.

Structure Description

The structure of ZASP-PDZ adopts the conventional PDZ fold: it is a mixed α/β protein that folds into a β sandwich with six β strands and two α helices (Figure 3). All β strands form antiparallel sheets, with α1 following β3 and α2 preceding β6. The first and last β strands

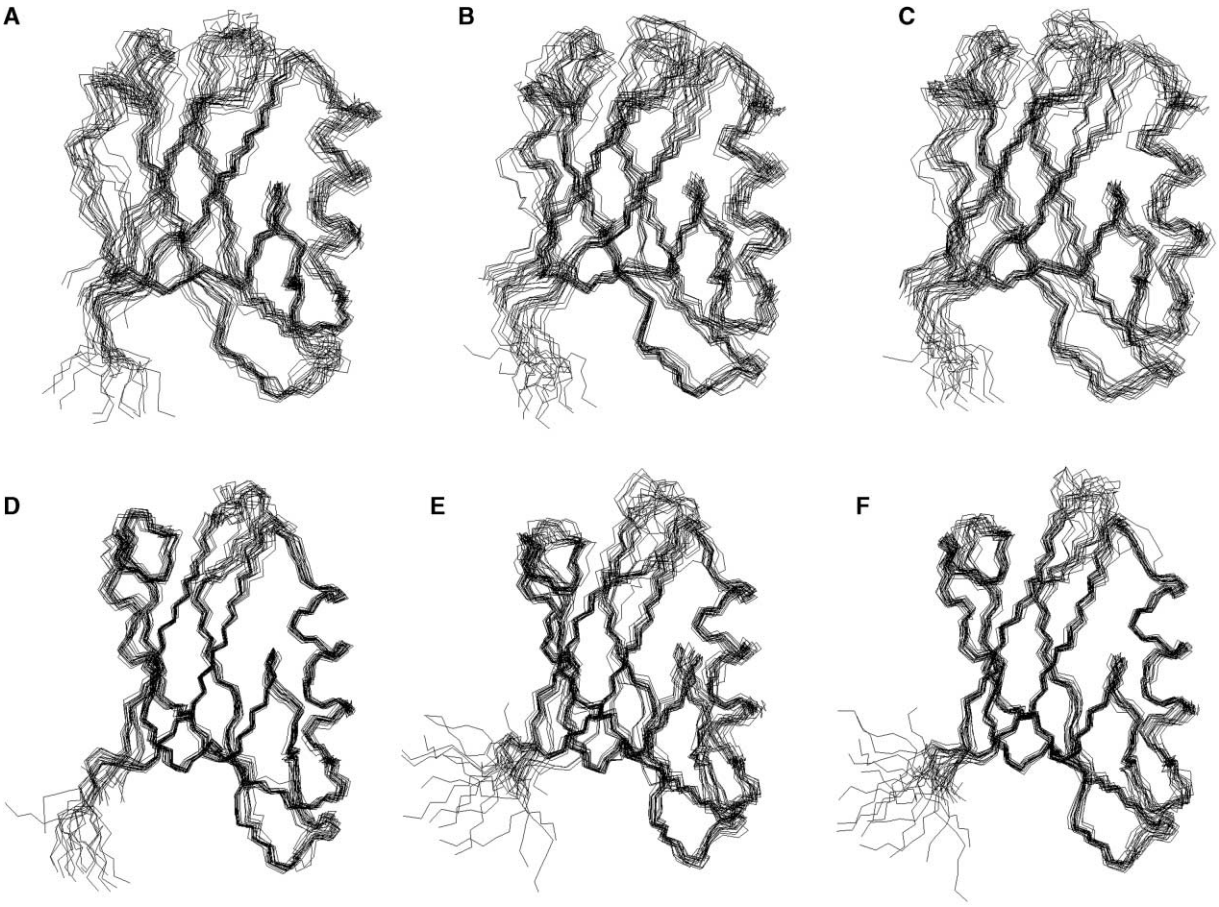

Figure 3. Structure Bundles of ZASP-PDZ

NMR bundles corresponding to the manually (top row) and automatically (bottom row) assigned structure families. From left to right are displayed the bundles without refinement (A and D), with RDC (B and E), and water refinement (C and F) respectively. No accepted structures contain distance violations >0.5 Å and/or no dihedral angle violations >5° from the experimental data.

(β1 and β6) form an antiparallel β sheet, on the opposite side of the β2-β3 antiparallel β sheet and α2, with β4 going across these structural elements. The groove between β2 and α2 which starts from the "GLGF" loop (residues P9, W10, G11, and F12 in ZASP-PDZ) and ending at the C-terminal portion of β2 is the conventional site of interaction for class 1 PDZ binding partners. In ZASP-PDZ, this pocket is delimited by the unique tryptophan at the N-terminal end of β2.

Binding of ZASP to α-Actinin-2

The affinity of the interaction between ZASP-PDZ and α-actinin-2 was measured by following the fluorescence signal of the unique tryptophan of ZASP-PDZ upon interaction with α-actinin-2. Act-EF34, containing the last two EF-hands of α-actinin-2, was first titrated against ZASP-PDZ yielding a K_d of 35.8 ± 5.3 μM. When Act-EF34 was first saturated with tZr7, titration against ZASP-PDZ yielded a K_d of 31.6 ± 3.8 μM: tZr7 is a 23 residue synthetic peptide spanning the sequence of titin's seventh Z-repeat, containing the region of interaction observed in the structure of Act-EF34/Zr7 complex (Atkinson et al., 2001). Since these values are the same within experimental error, we must conclude that the binding affinity is not modulated by the presence of tZr7 (Figure 5A).

To identify the residues involved in the ZASP-PDZ/Act-EF34 interaction, the two components were titrated individually. On titrating unlabeled ZASP-PDZ against ^{15}N-labeled Act-EF34, ^{15}N-HSQC spectra reveal chemical shift changes that confirm that ZASP-PDZ interacts with α-actinin-2, with most of the changes in the intermediate exchange regime. A plot of the weighted chemical shift variations versus residue number (Figure 5B) localizes changes to the Act-EF34 C terminus. Residues A61, S64, Y68, G69, D72, and L73 have the largest variations (>0.5). Similar results were obtained on titrating using the longer ^{15}N-labeled Act-EF1234 construct (data not shown). No appreciable effects could be observed involving residues from EF-hands 1 and 2. When the Act-EF34/tZr7 complex was formed prior to titration, similar but generally smaller variations were observed. This effect might be related to the conformational rearrangement that Act-EF34 undergoes upon binding the peptide (Atkinson et al., 2001): when already locked in a defined conformation, further complexation may cause smaller chemical shift perturbation.

On titrating unlabeled Act-EF1234 or Act-EF34 against

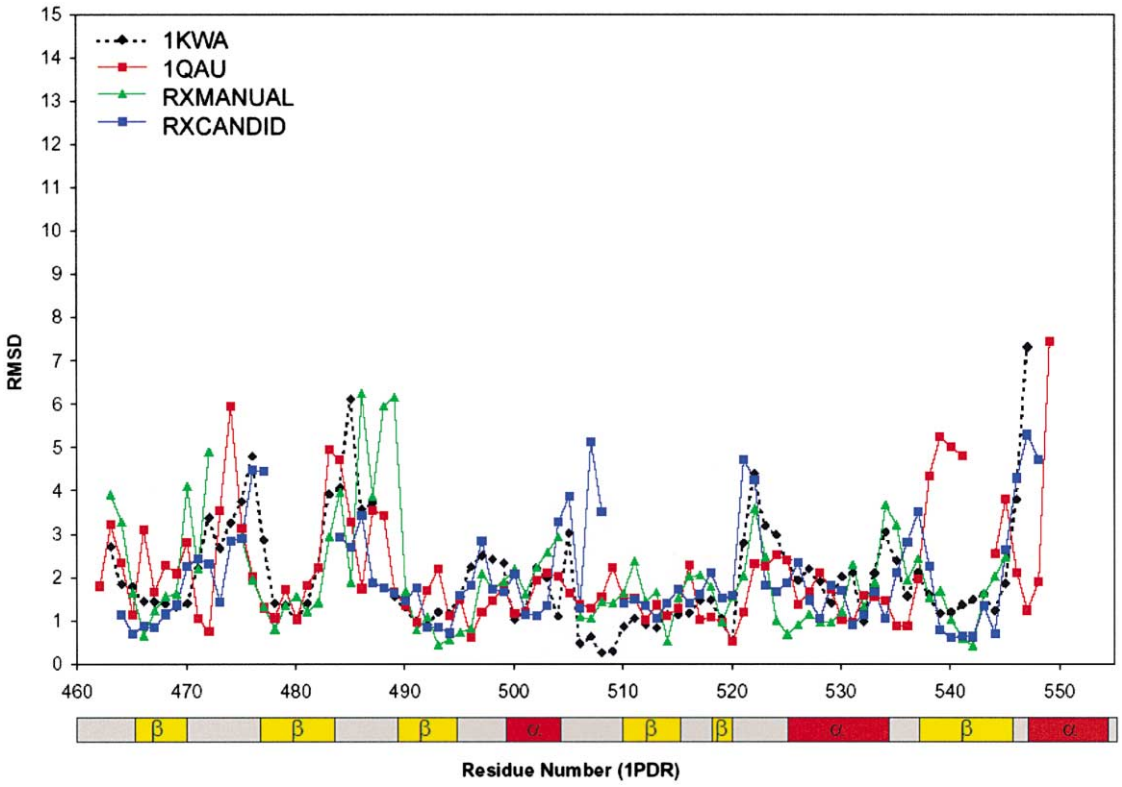

Figure 4. Rmsd Comparison of Known PDZ Structures with 1PDR

Pairwise comparison of the manually and automatically assigned bundles, 1kwa and 1qav structures with 1pdr, taken as a reference. The pairwise Z scores as obtained by WHATIF MOTIF option are plotted versus the sequence of 1pdr. The secondary structure elements of 1pdr are indicated underneath with yellow (β strands) and red (α helices) boxes.

Table 2. Structure Quality Indicators of ZASP-PDZ Bundles

	MANUAL	XMANUAL	RXMANUAL	CANDID	XCANDID	RXCANDID
Rmsd from mean (Å)						
Overall backbone	1.11	1.10	1.10	0.63	1.05	0.91
Overall heavy atom	1.73	1.65	1.66	1.23	1.54	1.47
Ordered backbone[a]	0.88	0.92	0.93	0.49	0.65	0.54
Ordered heavy atom	1.41	1.35	1.37	0.95	0.97	0.90
Structure Z scores						
First generation packing quality	−3.987	−3.903	−4.786	−1.853	−3.151	−2.872
Second generation packing quality	−4.228	−5.854	−5.787	−2.948	−4.028	−2.941
Ramachandran plot	−4.173	−5.636	−4.820	−3.342	−5.499	−3.217
Chi-1/chi-2 rotamer normality	−4.433	−4.851	−3.090	−4.509	−4.981	−2.943
Backbone conformation	−5.106	−2.316	−3.382	−3.579	−3.446	−2.003
Rms Z scores						
Bond lengths	0.444	0.944	1.023	0.443	0.950	1.024
Bond angles	0.955	1.388	1.307	0.954	1.375	1.283
Omega angle restraints	0.022	0.135	1.689	0.000	0.177	1.401
Side chain planarity	0.023	0.046	1.173	0.025	0.039	1.284
Improper dihedral distribution	0.615	0.966	0.994	0.614	0.963	0.993
Inside/outside distribution	1.082	1.063	1.045	1.066	1.040	1.034
Ramachandran plot						
Most favored regions (%)	70.9	72.5	76.3	73.8	65.1	81.6
Additional allowed regions (%)	25.7	22.9	19.8	24.3	31.6	16.8
Generously allowed regions (%)	2.8	3.7	2.5	1.1	2.5	1.3
Disallowed regions (%)	0.6	0.8	1.3	0.8	0.8	0.3

[a] The structures were superimposed using the backbone atoms of residues in secondary structures (3–7, 9–10, 12, 15–30, 32–37, 39–58, 60–72, and 76–82).

A

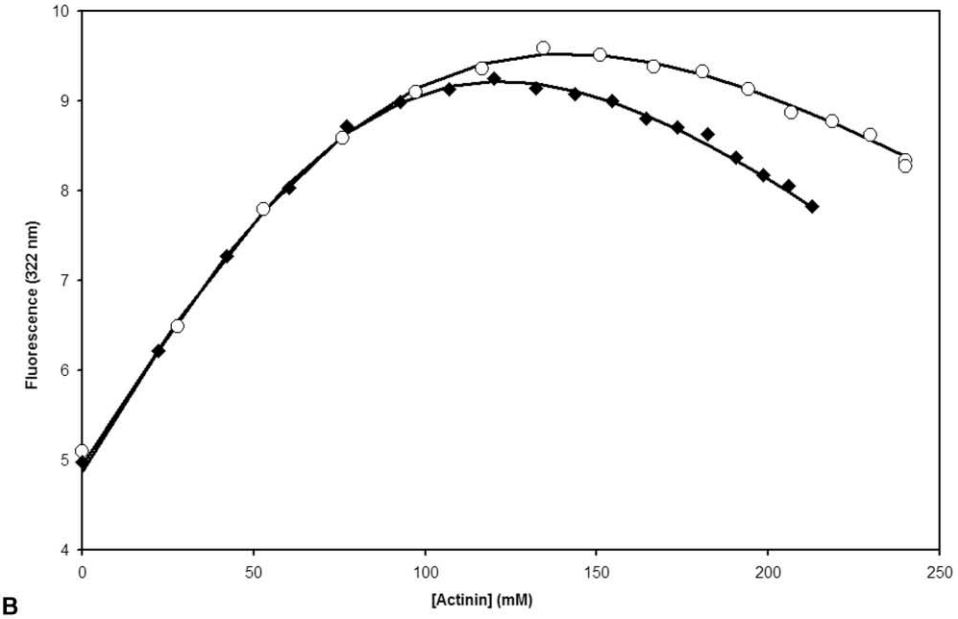
Fluorescence (322 nm)
[Actinin] (mM)

B

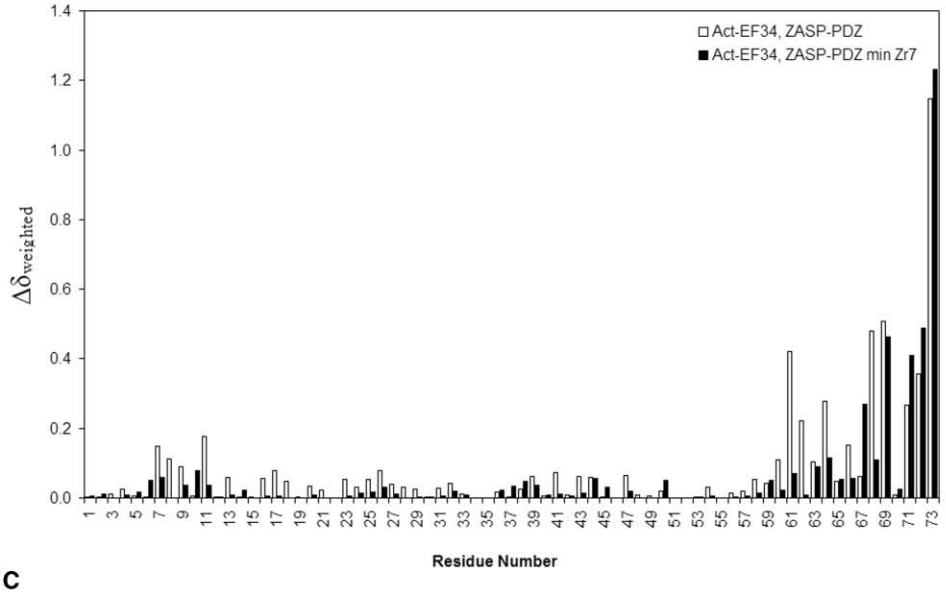
Act-EF34, ZASP-PDZ
Act-EF34, ZASP-PDZ min Zr7
Δδweighted
Residue Number

C

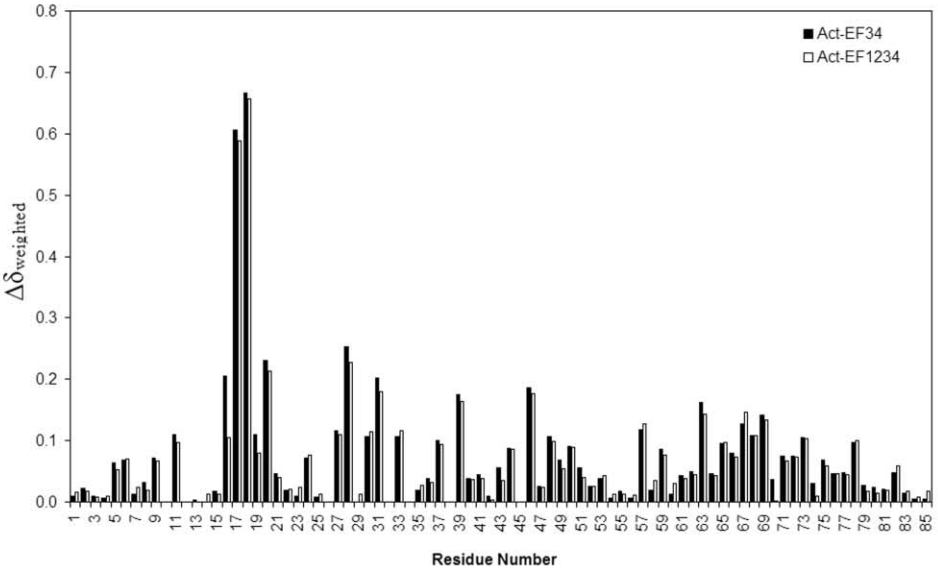
Act-EF34
Act-EF1234
Δδweighted
Residue Number

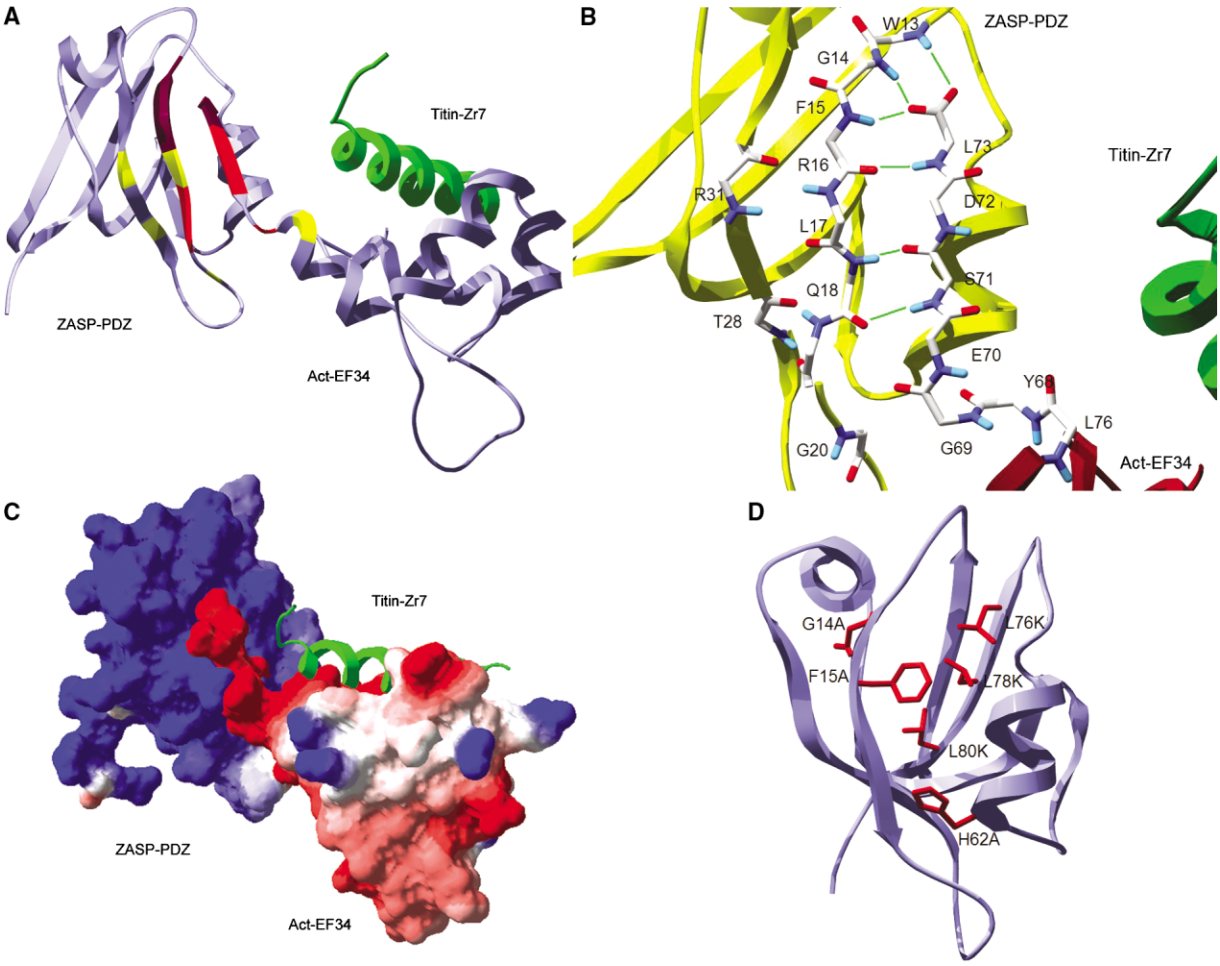

Figure 6. Model of the ZASP-PDZ/Act-EF34/Titin-ZR7 Complex and ZASP-PDZ Mutants

(A) Ribbon representation of the Act-EF34/tZr7/ZASP-PDZ ternary complex. The mutual orientation of Act-EF34 and ZASP-PDZ was chosen arbitrarily to avoid clashes between the two molecules. The observed chemical shift variations are reported on the structures: in purple are residues in intermediate exchange rate, in red and yellow are indicated chemical shift variations over 0.3 and 0.2 respectively (see Figure 5). Titin Zr7 is colored in green.

(B) Hydrogen bond network between ZASP-PDZ and Act-EF34 in the complex.

(C) Connolly surface representation (probe radius of 1.4 Å) of the trimeric complex, showing electrostatic complementarity.

(D) Mapping of point mutations described in (Zhou et al., 2001) onto the structure of ZASP-PDZ.

^{15}N-labeled ZASP-PDZ, the largest variations localize to a defined area of ZASP-PDZ around the "GLGF" motif and the second β strand. Residues W13, G14, and F15 are in intermediate exchange in the presence of Act-EF1234 (Figure 5C). Residues L17 and Q18 showed large chemical shift variations of around 6 ppm in the ^{15}N dimension.

From these data we conclude that the interaction between ZASP-PDZ and α-actinin-2 involves the groove between the β2 and the α2 and therefore belongs to the class 1 type. Although the binding affinity is relatively weak, it is well within the range observed for other PDZ domains (Hung and Sheng, 2002). Higher affinity might be achieved in muscle either through the contribution of other regions of ZASP or by further interactions of ZASP-PDZ with other muscle components.

Modeling of the Titin/α-Actinin-2/ZASP Ternary Complex

Despite attempts made to solve the structure of the complex directly by NMR, we could not detect any intermolecular NOE effects, probably due to the low binding

Figure 5. Effects of the Titration between Combinations of ZASP-PDZ with α-Actinin-2 and Titin Constructs

(A) Fluorescence titration of ZASP-PDZ against Act-EF34 (black diamonds), and the Act-EF34/tZr7 complex (white open circles).

(B) Chemical shift variations of the spectrum of ^{15}N-labeled Act-EF34 upon titration with unlabeled ZASP-PDZ plotted versus the Act-EF34 residue number. The data are reported for the titration of isolated Act-EF34 (white) and of Act-EF34 complexed tZr7 (black).

(C) Chemical shift variations of the spectrum of ^{15}N-labeled ZASP-PDZ upon titration with unlabeled Act-EF1234 (white) or Act-EF34 (black) plotted versus the ZASP-PDZ sequence.

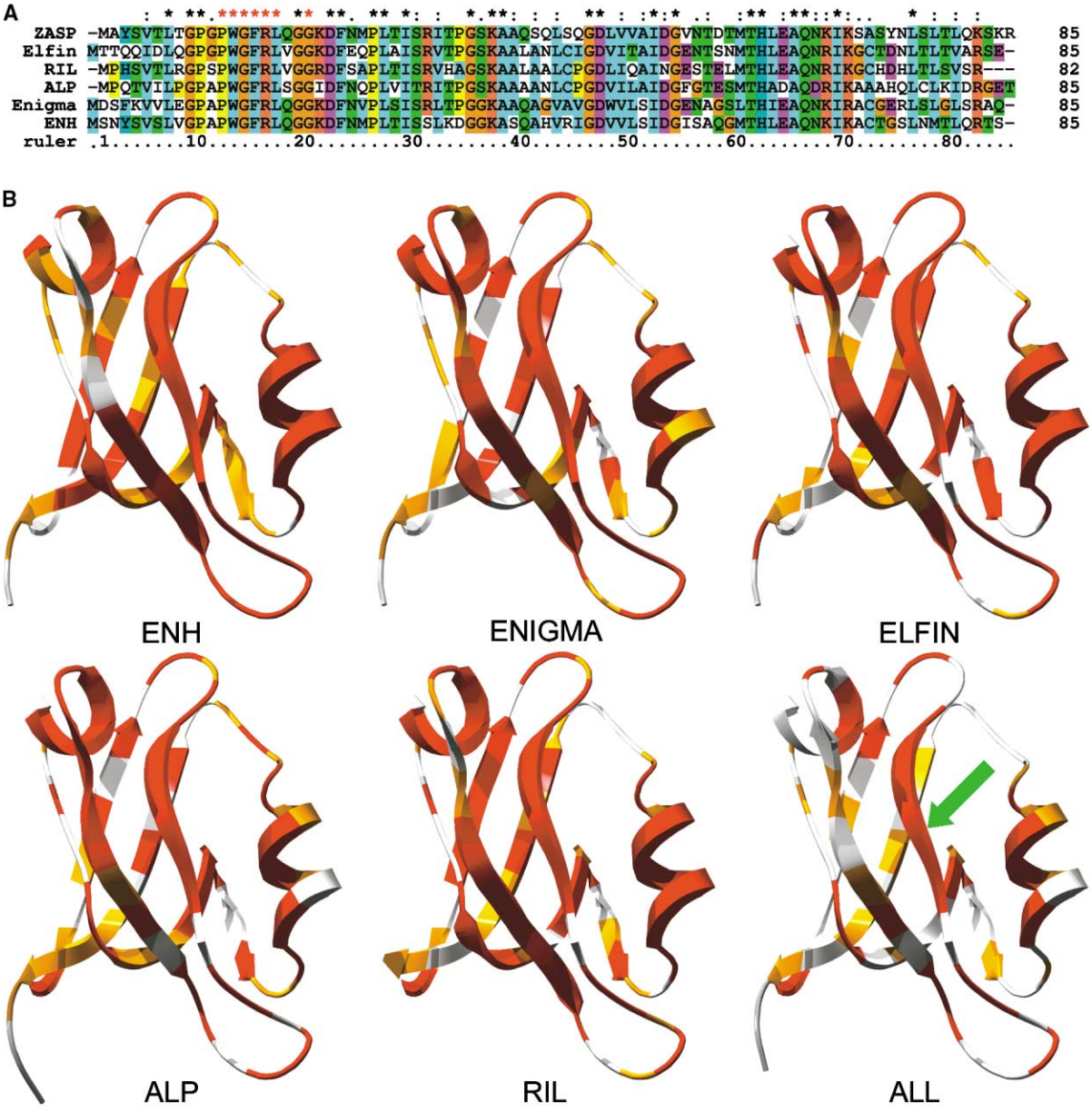

Figure 7. Enigma Family PDZ Domain Homology Models

(A) Sequence alignment of the PDZ domains of the enigma family. The numbering refers to ZASP. Stars, semicolons, and dots denote decreasing levels of conservation. Red stars are used for the residues most affected by binding (see Figure 5B).

(B) Comparative models of other PDZ domains from the enigma family. Highlighted red, orange, and yellow residues correspond to identical positions and decreasing levels of similarity of the sequence in a pairwise comparison with ZASP-PDZ. White are nonconserved residues. The sequence conservation across the whole family is mapped on the structure marked "ALL." A green arrow indicates the strand involved in α-actinin-2 binding.

affinity. The Act-EF34/tZr7/ZASP-PDZ complex was therefore modeled using as templates a class 1 PDZ domain bound to its target peptide (1be9 [Doyle et al., 1996]) and the structure of the Act-EF34/tZr7 complex (1h8b [Atkinson et al., 2001]). Interestingly, the Zr7 and ZASP-PDZ binding sites occupy distinct regions of the Act-EF34 structure, thus making it possible for both interactions to occur simultaneously (Figure 6A).

Inspection of the ternary complex reveals six possible intermolecular hydrogen bonds between Act-EF34 and ZASP-PDZ (Figure 6B). W13, G14, and F15 backbone amides of ZASP-PDZ could form a hydrogen bond network with the C-terminal carboxylate group of Act-EF34. F15 backbone carboxy group pairs with the 0 position (L73) backbone amide. L17 carboxy and amide backbone groups pair with the -2 position (S71) backbone amide and carboxy group respectively. The ZASP-PDZ side chains of W13, G14, and F15 can form a hydrophobic cluster with L73 of Act-EF34, whose amide proton could be ring current shifted by the proximity of W13

thus explaining the appreciable chemical shift variation observed (Figure 5C). R16 and H62 can form electrostatic interactions with positions −1 (D72) and −3 position (E70) respectively. H62, important for target specificity (Doyle et al., 1996), can in principle also form hydrogen bond with the side chain of S71. Q66 forms a polar interaction with the −2 position (S71).

The electrostatic potential at pH 7 of ZASP-PDZ and Act-EF34 was calculated and mapped onto the Connolly surface of the model (Figure 6C). This shows a strong charge complementarity around the binding surface with the highly positively charged ZASP-PDZ (the construct has an isoelectric point of 9.78) interacting with the negatively charged C terminus of Act-EF34 (isoelectric point of 4.34).

Our results allow us to interpret and rationalize the elegant work by Chen and coworkers (Zhou et al., 2001) who explored the effects of ZASP PDZ point mutations on α-actinin-2 binding. A G14A/F15A double mutation abolished completely α-actinin-2 binding (Figure 6D). The importance of these residues for binding is in agreement with the results of the titrations described above. Single mutation of L76K, L78K, and L80K located on the opposite side of the binding groove also decreased binding significantly. As part of the hydrophobic core, the mutation of these residues is likely to disrupt the PDZ fold. Mutation of H62 into an alanine caused only a marginal decrease of binding. The side chain of H62 could form a hydrogen bond with the ligand, in which case it would contribute to the affinity but might not be essential for the formation of the complex.

Therefore, the picture that emerges from this study is that the PDZ domain of ZASP constitutes an important anchorage point of this protein to the Z disk, making it an integral part of the highly complex mesh of interactions that form the scaffold necessary for muscle contraction.

Homology Modeling of the Enigma Family of PDZ

Finally, ZASP-PDZ was used to model by homology other members of the enigma family that have a pairwise sequence identity with it varying between 54%–61% and sequence similarity between 71%–81%. A blast search (Altschul et al., 1997) using the ZASP PDZ sequence recovered 50 sequences. After discarding nonmammalian and hypothetical protein sequences and eliminating the redundancies, the remaining PDZ sequences identify six subgroups: ZASP, enigma, ENH, RIL, ALP, and elfin (Figure 7A). These proteins are all known to be expressed in mammalian heart and/or striated muscle with the exception of RIL, which has only been detected in epithelial tissue (Cuppen et al., 1998). One representative sequence per group was homology modeled.

The resulting models may help to identify structurally or functionally relevant residues across the enigma family (Figure 7B). Interestingly, the most conserved residues are not those involved in the hydrophobic core of the protein but those close to the binding groove, such as G9, W13-L17, G20, D22, F23, H62, A65, Q66, and I69. Other conserved residues, although not directly involved in the interaction, might be relevant for the binding: K37 and A38, for instance, may stabilize the orientation of the "GLGF" loop. The pattern of sequence conservation compares well with the residues most affected in our titrations. The only exception is Q18, which experiences large chemical shift changes upon complex formation but is not well conserved. This residue, although described to make only minor Van der Waals contacts with the target, can be expected to experience a large variation of the chemical environment being directly contiguous to the target (Doyle et al., 1996).

Conservation of the residues of ZASP PDZ involved in α-actinin-2 recognition would therefore suggest that this function is maintained in the whole family. In contrast, the literature is rather contradictory on this point: ZASP, ENH, and ALP have been described to bind α-actinin-2, except that ALP was reported to recognize the α-actinin-2 spectrin-like domains (Xia et al., 1997). Enigma has been reported to bind β-tropomyosin, but not α-actinin (Guy et al., 1999). The information about elfin (also called hCLIM1, CLP-36, and hCLP-36) is even more confusing. hCLIM1 is thought to bind α-actinin-2 via its LIM domains, hCLP36 binds to α-actinin-1 via the intervening sequence between the PDZ and LIM domain, whereas CLP-36 binds α-actinin-1 and α-actinin-4 via its PDZ domain (Bauer et al., 2000; Kotaka et al., 2000, 2001; Vallenius et al., 2000). Based on our results and the pattern of sequence conservation, we predict that all currently known members of the family are able to bind α-actinin-2 in vitro. It is possible that in vivo other regions of the proteins intervene in a family-member-specific fashion to modify the signaling properties of the Z disk through the interaction with other components such as calsarcins and other Z disk proteins (Frey and Olson, 2002). Further studies will be necessary to test these hypotheses and to assess further the reasons for redundancy of the enigma protein family.

Experimental Procedures

Protein Expression and Purification

The constructs span the human sequences of skeletal muscle ZASP-PDZ (residues 1–85) and α-actinin-2 (residues 745–894 and 823–894 for Act-EF1234 and Act-EF34 respectively) (EMBL/GenBank accession codes Q9Y4Z5 and M86406, respectively). For purification purposes, all constructs were expressed as six-histidine tag (6HIS) and *S. Japonicum* glutathion-S-transferase fusion proteins (GST) using a 7 residue recombinant tobacco endovirus (rTEV) protease recognition site to separate 6HIS-GST from the protein of interest. The proteins were expressed using a pET9d plasmid that conferred kanamycin resistance and transformed in *E. Coli* BL21(DE3) or BL21(DE3)pLysS competent cells (Novagen). A Luria-Bertani (LB) broth containing kanamycin (30 μg/ml) was used to select and grow the transformed cells, incubating at 37°C. The cells were induced by adding isopropyl β-D-thiogalactopyranoside IPTG (0.5 mM) when the optical density at 595 nm was 0.5–0.6 and allowing the cells to incubate at 37°C for an additional 3 hr. ^{15}N-labeled or ^{15}N/^{13}C labeled proteins were produced by growing the bacteria in minimal media using ^{15}N-ammonium sulfate and ^{13}C-glucose as the sole nitrogen or carbon sources, as appropriate.

Cells were pelleted by centrifugation (Beckman) and subsequently resuspended in lysis buffer (20 mM Tris-HCl [pH 8], 200 mM NaCl, 5 mM imidazole, 0.2% v/v IPEGAL CA-630, lysozyme, DNase I, Protease Inhibitor Cocktail [Roche]), using 25 ml/l growth of cells. The cells were then sonicated (MODEL) and the supernatant was collected after centrifugation. The 6HIS-GST-TEV fusion protein was purified from the cell extract by Ni-NTA agarose column (QIAGEN), and incubated with TEV protease (GIBCO-BRL) overnight at room temperature. The target protein was then purified from the cleaved

6HIS-GST by gel filtration using a Pharmacia Superdex 75 16/60 column (20 mM Tris-HCl [pH 8], 200 mM NaCl buffer). Protein samples were then buffer exchanged using a Sephadex G-25M PD-10 column into 20 mM Na_2PO_4, 0.02% NaN_3, pH 6.6, with the addition of D_2O for a final v/v concentration of 10%. Typical protein concentrations for NMR samples were approximately 0.5 mM as determined by measuring UV absorbance at 280 nm.

Solid-Phase Peptide Synthesis and Purification

The tZr7 peptide (GKKAEAVATVVAAVDQARVREPR) was synthesized using standard solid-phase synthesis techniques (Atherton and Sheppard, 1989) with a Milligen 9050 synthesizer. Protected amino acids and chemicals were purchased from Bachem, Novabiochem, or Fluka (Switzerland). The resin loaded with glutamic acid (Fmoc-Glu(OBut)-PEG-PS) from Millipore (Waltham, MA) (0.5 g) was treated with piperidine (20%) in DMF. The N^{α}-Fmoc amino acid derivatives were sequentially coupled to the growing peptide chain by using a 4-fold excess of [O-(7-azabenzotriazol-1-yl)-1,1,3,3-tetramethyluronium hexafluorophosphate] (HATU [Carpino, 1993]) in DMF. Piperidine (20%) in DMF was used to remove the Fmoc group at all steps. The protected peptide-PEG-PS-resin was cleaved from the resin by treatment with TFA/H_2O/phenol/ethanedithiol/thioanisole (reagent K) (82.5: 5: 5: 2.5: 5; v/v) (King et al., 1990).

Crude peptide was purified by preparative reversed-phase HPLC using a Water Delta Prep 4000 system with a Waters PrepLC 40 mm Assembly column C18 (30 $\times$ 4 cm, 300 Å, 15 mm spherical particle size column) using a linear gradient from 10% to 40% of acetonitrile in 0.1% TFA. The molecular weight of the compound was confirmed by a matrix-assisted laser desorption ionization time of flight (MALDI-TOF) analysis using a Hewlett Packard G2025A LD-TOF system mass spectrometer.

NMR Data Acquisition and Processing

All spectra were recorded at 27°C, using 500 or 600 MHz (^{1}H frequency) Varian spectrometers equipped with 5 mm triple-resonance probes. The WATERGATE sequence was used for water suppression (Piotto et al., 1992). Two-dimensional ^{1}H-^{1}H TOCSY and NOESY experiments and hetero-nuclear ^{15}N-HSQC, ^{13}C-HSQC, HNCA, HN(CO)CA, HNCO, CBCA(CO)NH, CBCANH, HCCH-TOCSY, and ^{15}N-TOCSY-HSQC were acquired for ZASP-PDZ assignment (Cavanagh et al., 1996). Typical mixing times for the TOCSY and NOESY were between 50 and 100 ms.

The spectra were processed using NMRPipe (Delaglio et al., 1995) and analyzed using XEASY software (Bartels et al., 1995). Typically, the acquisition dimension was multiplied by a Gaussian function, whereas a 90° shifted sine-bell function was applied to the indirect dimensions. Each dimension was zero filled to the next appropriate power of two.

Assignment of ZASP-PDZ

Virtually complete assignment of the ^{1}H, ^{15}N, and ^{13}C resonances was obtained for unbound ZASP-PDZ using CBCACONH, CBCANH, HNHA, HNCO, ^{1}H-^{15}N TOCSY-HSQC, and HCCH-TOCSY spectra. All backbone atoms were assigned, with the exception of the backbone carbonyl resonances that are followed by a proline. All side chain resonances were assigned, except for the ^{1}H resonances of the N-terminal methionine, ^{13}C resonances of the aromatic side chains past their Cβ, ^{13}C resonances for L7 and H62 past their Cβ, ^{13}C and ^{1}H resonances for P12, and most exchangeable side chain protons.

Assignment of the resonances of complexed ZASP-PDZ was facilitated by titration, allowing the transfer of 94% of the backbone amide assignments. These were confirmed by comparing ^{15}N-edited TOCSY and NOESY spectra of the complex with those of unbound ZASP-PDZ. Residues 13–18 of ZASP-PDZ were broadened by chemical exchange upon complex formation. Although it was possible to follow their amide resonances in the titration, their side chain ^{1}H resonances could not be observed. Proline residues 10, 12, 26, and 34 and other side chain assignments could not be completed, leading to the ^{1}H and ^{15}N assignment to be 76% of that of unbound ZASP-PDZ.

Structure Calculation

Distance restraints were obtained from three-dimensional ^{1}H-^{15}N NOESY-HSQC, ^{1}H-^{13}C NOESY-HSQC, and two-dimensional ^{1}H-^{1}H NOESY spectra with mixing times of 50, 100, and 100 ms respectively. NOE peak volumes were calculated with the program SPSCAN (http://www.molebio.uni-jena.de/~rwg/spscan) using five iterations of integration and converted into interproton upper-limit distance restraints by the programs CALIBA (Guntert et al., 1997). Angular (ϕ and ψ) restraints were obtained from TALOS (Cornilescu et al., 1999) and/or from HNHA spectra. H bonds were measured from HNCO spectra (Cordier and Grzesiek, 1999). The ZASP-PDZ NMR sample was partially aligned using penta(ethylene) glycol monododecyl ether (C12E5) and n-hexanol. The surfactant/water ratio was 5% (w/v) and the molar ratio of surfactant/alcohol was 0.96 M ratio (Ruckert and Otting, 2000). RDCs were determined with an HSQC-IPAP experiment (Ottiger et al., 1998). Only backbone amide RDC restraints for protons whose T1/T2 ratios were not outside 1 standard deviation from the mean or whose backbone amide NOE value was greater than 0.7 were considered. Stereospecific assignments were achieved by the program GLOMSA (Guntert et al., 1991).

The structures were first calculated using two different protocols. In the MANUAL run, structure calculation was achieved by CYANA (Guntert et al., 1997) and based on manually assigned distance restraints, hydrogen bonds, and dihedral angles information. The simulated annealing protocol involved a high-temperature conformational search stage of 2000 steps, followed by slow cooling over 8000 steps with conjugate gradient minimization at the end. The redundant dihedral angle (REDAC [Guntert and Wuthrich, 1991]) strategy was used to help structure convergence, typically using 5 cycles of 100 structures. The final set of distance restraints was obtained by an iterative procedure using converged structures to assist the assignment of ambiguous NOEs.

For the second run we used the program CANDID (Herrmann et al., 2002) to achieve automatic assignment. The default run of seven cycles was used. This method was of course faster, but the algorithm could not converge to the correct PDZ fold without dihedral angles and hydrogen bonds. To circumvent the problem, we added to the hydrogen bonds observed in the HNCO those inferred from the MANUAL bundle. After initial testing, we also noticed that, due to the higher intrinsic resolution, convergence was better if using only the homonuclear ^{1}H-^{1}H NOESY. Using this strategy, only few long-range restraints (22) would be left out.

Both sets of structures were successively refined against RDC using XPLOR (Schwieters et al., 2003) and finally improved by using the "CHARMM22 water-refinement protocol" as detailed in (Spronk et al., 2002).

Fluorescence

Dissociation constants of the interaction of ZASP or ZASP/tZr7 with Act-EF34 were obtained by monitoring the intensity of the fluorescence emitted by the single tryptophan of ZASP-PDZ. The spectra were detected at 20°C in 20 mM phosphate (pH 6.6). A SPEX FluoroMax fluorimeter was used with excitation at 295 nm and emission intensity recorded at 322 nm. Dissociation constants were obtained by nonlinear regression analysis relating the change in fluorescence intensity at 322 nm to the total added concentration through the following equation: $F = (F_o + F_{max}[L]/K_d)/(1 + [L]/K_d)$, where the F, F_o, and F_{max} are fluorescence intensities measured at each titration point, at zero ligand concentration, and at saturation respectively, and [L] is the concentration of free ligand calculated by the quadratic equation:

$$[L]^2 - [L]([P_o] - [L_o] + K_d) - K_d [L_o] = 0,$$

where $[P_o]$ and $[L_o]$ are the protein and ligand added concentrations respectively.

^{15}N-HSQC Titration

The unlabeled protein was added using molar ratios from 10:1 to 1:2 (or until no further spectral changes were observed) to its ^{15}N-labeled partner, acquiring the ^{15}N HSQC spectrum for each addition. ^{15}N HSQC spectra typically acquired using 2400 and 64 points in the direct and indirect dimensions respectively. The weighted chemical shift variation was calculated for each peak using the following equation:

$$\Delta\delta_{weighted} = \sqrt{\Delta\delta_{1H}^2 + \left(\frac{\Delta\delta_{15N}}{10}\right)^2},$$

in which $\Delta\delta_{1H}$ and $\Delta\delta_{15N}$ are the chemical shift variations in the proton and nitrogen dimensions respectively.

Bioinformatics and Homology Modeling

Sequence alignments were obtained and displayed by ClustalX (Thompson et al., 1997). The DALI server was used to find similar protein structures (Holm and Sander, 1996a). Modeling of the ternary complex was achieved by the following procedure: first, the last four residues of Act-EF34 were rebuilt in an extended conformation compatible with class 1 PDZ recognition. Second, ZASP-PDZ was superimposed onto the structure of 1be9, using the regions of maximal superposition as indicated by DALI (Holm and Sander, 1996b). Finally, the last four residues of Act-EF34 were aligned with the interacting peptide in 1be9 so that L73 of Act-EF34 would superimpose with the C-terminal residue of the peptide. The final structure was then submitted to 200 cycles of constrained energy minimization using the standard protocol within SWISS-PDB Viewer (GROMOS 43B1 force field). Homology modeling of PDZ homologs was based on the ClustalX alignment and performed using SWISS-MODEL in combination with Swiss PDB Viewer (Guex and Peitsch, 1997). The coordinates of the models are available from the authors upon request. The electrostatic potential was calculated by the SWISS-MODEL Viewer.

Acknowledgments

The authors wish to thank T. Frenkiel of the MRC Biomedical NMR Centre, NIMR for technical assistance. The financial support of Telethon-Italy to G.F. (Grant 1278) is gratefully acknowledged.

Received: November 18, 2003
Revised: December 30, 2003
Accepted: January 8, 2004
Published: April 6, 2004

References

Altschul, S.F., Madden, T.L., Schaffer, A.A., Zhang, J.H., Zhang, Z., Miller, W., and Lipman, D.J. (1997). Gapped BLAST and PSI-BLAST: a new generation of protein database search programs. Nucleic Acids Res. *25*, 3389–3402.

Atherton, E., and Sheppard, R.C. (1989). Solid Phase Peptide Synthesis: A Practical Approach (New York: Oxford University Press).

Atkinson, R.A., Joseph, C., Kelly, G., Muskett, F.W., Frenkiel, T.A., Nietlispach, D., and Pastore, A. (2001). Ca2+-independent binding of an EF-hand domain to a novel motif in the alpha-actinin-titin complex. Nat. Struct. Biol. *8*, 853–857.

Bartels, C., Xia, T.-H., Billeter, M., Guntert, P., and Wuthrich, K. (1995). The program XEASY for computer-supported NMR spectral analysis of biological macromolecules. J. Biomol. NMR *5*, 1–10.

Bauer, K., Kratzer, M., Otte, M., de Quintana, K.L., Hagmann, J., Arnold, G.J., Eckerskorn, C., Lottspeich, F., and Siess, W. (2000). Human CLP36, a PDZ-domain and LIM-domain protein, binds to alpha-actinin-1 and associates with actin filaments and stress fibers in activated platelets and endothelial cells. Blood *96*, 4236–4245.

Beggs, A.H., Byers, T.J., Knoll, J.H.M., Boyce, F.M., Bruns, G.A.P., and Kunkel, L.M. (1992). Cloning and characterization of 2 human skeletal-muscle alpha-actinin genes located on chromosome-1 and chromosome-11. J. Biol. Chem. *267*, 9281–9288.

Bowles, K.R., Abraham, S.E., Brugada, R., Zintz, C., Comeaux, J., Sorajja, D., Tsubata, S., Li, H., Brandon, L., Gibbs, R.A., et al. (2000). Construction of a high-resolution physical map of the chromosome 10q22- q23 dilated cardiomyopathy locus and analysis of candidate genes. Genomics *67*, 109–127.

Carpino, L.A. (1993). 1-hydroxy-7-azabenzotriazole—an efficient peptide coupling additive. J. Am. Chem. Soc. *115*, 4397–4398.

Cavanagh, J., Fairbrother, W.J., Palmer, A.G., III, and Skelton, N.J. (1996). Protein NMR Spectroscopy: Principals and Practice (San Diego, CA: Academic Press).

Clark, K.A., McEthinny, A.S., Beckerle, M.C., and Gregorio, C.C. (2002). Striated muscle cytoarchitecture: an intricate web of form and function. Annu. Rev. Cell Dev. Biol. *18*, 637–706.

Cordier, F., and Grzesiek, S. (1999). Direct observation of hydrogen bonds in proteins by interresidue (3h)J(NC′) scalar couplings. J. Am. Chem. Soc. *121*, 1601–1602.

Cornilescu, G., Delaglio, F., and Bax, A. (1999). Protein backbone angle restraints from searching a database for chemical shift and sequence homology. J. Biomol. NMR *13*, 289–302.

Cuppen, E., Gerrits, H., Pepers, B., Wieringa, B., and Hendriks, W. (1998). PDZ motifs in PTP-BL and RIL bind to internal protein segments in the LIM domain protein RIL. Mol. Biol. Cell *9*, 671–683.

Delaglio, F., Grzesiek, S., Vuister, G.W., Zhu, G., Pfeifer, J., and Bax, A. (1995). NMRPipe: a multidimensional spectral processing system based on UNIX pipes. J. Biomol. NMR *6*, 277–293.

Doyle, D.A., Lee, A., Lewis, J., Kim, E., Sheng, M., and MacKinnon, R. (1996). Crystal structures of a complexed and peptide-free membrane protein- binding domain: molecular basis of peptide recognition by PDZ. Cell *85*, 1067–1076.

Faulkner, G., Pallavicini, A., Formentin, E., Comelli, A., Ievolella, C., Trevisan, S., Bortoletto, G., Scannapieco, P., Salamon, M., Mouly, V., et al. (1999). ZASP: a new Z-band alternatively spliced PDZ-motif protein. J. Cell Biol. *146*, 465–475.

Faulkner, G., Lanfranchi, G., and Valle, G. (2001). Telethonin and other new proteins of the Z-disc of skeletal muscle. IUBMB Life *51*, 275–282.

Frey, N., and Olson, E.N. (2002). Calsarcin-3, a novel skeletal muscle-specific member of the calsarcin family, interacts with multiple Z disc proteins. J. Biol. Chem. *277*, 13998–14004.

Gerull, B., Gramlich, M., Atherton, J., McNabb, M., Trombitas, K., Sasse-Klaassen, S., Seidman, J.G., Seidman, C., Granzier, H., Labeit, S., et al. (2002). Mutations of TTN, encoding the giant muscle filament titin, cause familial dilated carddiomyopathy. Nat. Genet. *30*, 201–204.

Goodwin, J.F. (1982). The frontiers of cardiomyopathy. Br. Heart J. *48*, 1–18.

Guex, N., and Peitsch, M.C. (1997). SWISS-MODEL and the Swiss-PdbViewer: an environment for comparative protein modeling. Electrophoresis *18*, 2714–2723.

Guntert, P., and Wuthrich, K. (1991). Improved efficiency of protein structure calculations from NMR data using the program DIANA with redundant dihedral angle constraints. J. Biomol. NMR *1*, 446–456.

Guntert, P., Qian, Y.Q., Otting, G., Muller, M., Gehring, W., and Wuthrich, K. (1991). Structure determination of the Antp(C39-]S) homeodomain from nuclear-magnetic-resonance data in solution using a novel strategy for the structure calculation with the programs Diana, Caliba, Habas, and Glomsa. J. Mol. Biol. *217*, 531–540.

Guntert, P., Mumenthaler, C., and Wuthrich, K. (1997). Torsion angle dynamics for NMR structure calculation with the new program DYANA. J. Mol. Biol. *273*, 283–298.

Guy, P.M., Kenny, D.A., and Gill, G.N. (1999). The PDZ domain of the LIM protein enigma binds to beta-tropomyosin. Mol. Biol. Cell *10*, 1973–1984.

Herrmann, T., Guntert, P., and Wuthrich, K. (2002). Protein NMR structure determination with automated NOE assignment using the new software CANDID and the torsion angle dynamics algorithm DYANA. J. Mol. Biol. *319*, 209–227.

Hillier, B.J., Christopherson, K.S., Prehoda, K.E., Bredt, D.S., and Lim, W.A. (1999). Unexpected modes of PDZ domain scaffolding revealed by structure of nNOS-syntrophin complex. Science *284*, 812–815.

Holm, L., and Sander, C. (1996a). Alignment of three-dimensional protein structures: network server for database searching. Methods Enzymol. *266*, 653–662.

Holm, L., and Sander, C. (1996b). Mapping the protein universe. Science *273*, 595–602.

Hung, A.Y., and Sheng, M. (2002). PDZ domains: structural modules for protein complex assembly. J. Biol. Chem. *277*, 5699–5702.

Johnson, R.A., and Palacios, I. (1982). Dilated cardiomyopathies of the adult.1. N. Engl. J. Med. *307*, 1051–1058.

King, D.S., Fields, C.G., and Fields, G.B. (1990). A cleavage method which minimizes side reactions following Fmoc solid-phase peptide-synthesis. Int. J. Pept. Protein Res. *36*, 255–266.

Knoll, R., Hoshijima, M., Hoffman, H.M., Person, V., Lorenzen Schmidt, I., Bang, M.L., Hayashi, T., Shiga, N., Yakusawa, H., Schaper, W., et al. (2002). Cell *27*, 944–955.

Kotaka, M., Kostin, S., Ngai, S., Chan, K., Lau, Y., Lee, S.M., Li, H., Ng, E.K., Schaper, J., Tsui, S.K., et al. (2000). Interaction of hCLIM1, an enigma family protein, with alpha-actinin 2. J. Cell. Biochem. *78*, 558–565.

Kotaka, M., Lau, Y., Cheung, K., Lee, S.M., Li, H., Chan, W., Fung, K., Lee, C., Waye, M.M., and Tsui, S.K. (2001). Elfin is expressed during early heart development. J. Cell. Biochem. *83*, 463–472.

Morais Cabral, J.H., Petosa, C., Sutcliffe, M.J., Raza, S., Byron, O., Poy, F., Marfatia, S.M., Chishti, A.H., and Liddington, R.C. (1996). Crystal structure of a PDZ domain. Nature *382*, 649–652.

Ottiger, M., Delaglio, F., and Bax, A. (1998). Measurement of J and dipolar couplings from simplified two-dimensional NMR spectra. J. Magn. Reson. *131*, 373–378.

Piotto, M., Saudek, V., and Sklenar, V. (1992). Gradient-tailored excitation for single-quantum NMR- spectroscopy of aqueous-solutions. J. Biomol. NMR *2*, 661–665.

Ruckert, M., and Otting, G. (2000). Alignment of biological macromolecules in novel nonionic liquid crystalline media for NMR experiments. J. Am. Chem. Soc. *122*, 7793–7797.

Schwieters, C.D., Kuszewski, J.J., Tjandra, N., and Clore, G.M. (2003). The Xplor-NIH NMR molecular structure determination package. J. Magn. Reson. *160*, 65–73.

Sorimachi, H., Freiburg, A., Kolmerer, B., Ishiura, S., Stier, G., Gregorio, C.C., Labeit, D., Linke, W.A., Suzuki, K., and Labeit, S. (1997). Tissue-specific expression and alpha-actinin binding properties of the Z-disc titin: implications for the nature of vertebrate Z-discs. J. Mol. Biol. *270*, 688–695.

Spronk, C.A., Linge, J.P., Hilbers, C.W., and Vuister, G.W. (2002). Improving the quality of protein structures derived by NMR spectroscopy. J. Biomol. NMR *22*, 281–289.

Sugrue, D.D., Rodeheffer, R.J., Codd, M.B., Ballard, D.J., Fuster, V., and Gersh, B.J. (1992). The clinical course of idiopathic dilated cardiomyopathy: a population-based study. Ann. Intern. Med. *117*, 117–123.

Thompson, J.D., Gibson, T.J., Plewniak, F., Jeanmougin, F., and Higgins, D.G. (1997). The CLUSTAL_X windows interface: flexible strategies for multiple sequence alignment aided by quality analysis tools. Nucleic Acids Res. *25*, 4876–4882.

Vallenius, T., Luukko, K., and Makela, T.P. (2000). CLP-36 PDZ-LIM protein associates with nonmuscle alpha-actinin-1 and alpha-actinin-4. J. Biol. Chem. *275*, 11100–11105.

Walma, T., Spronk, C.A., Tessari, M., Aelen, J., Schepens, J., Hendriks, W., and Vuister, G.W. (2002). Structure, dynamics and binding characteristics of the second PDZ domain of PTP-BL. J. Mol. Biol. *316*, 1101–1110.

Xia, H., Winokur, S.T., Kuo, W.L., Altherr, M.R., and Bredt, D.S. (1997). Actinin-associated LIM protein: identification of a domain interaction between PDZ and spectrin-like repeat motifs. J. Cell Biol. *139*, 507–515.

Young, P., Ferguson, C., Banuelos, S., and Gautel, M. (1998). Molecular structure of the sarcomeric Z-disk: two types of titin interactions lead to an asymmetrical sorting of alpha-actinin. EMBO J. *17*, 1614–1624.

Zhou, Q., Chu, P.H., Huang, C., Cheng, C.F., Martone, M.E., Knoll, G., Shelton, G.D., Evans, S., and Chen, J. (2001). Ablation of Cypher, a PDZ-LIM domain Z-line protein, causes a severe form of congenital myopathy. J. Cell Biol. *155*, 605–612.

Accession Numbers

The assignments have been deposited with the BioMagResBank (http://www.bmrb.wisc.edu) with accession codes BMRB-5696 (unbound ZASP-PDZ) and BMRB-5697 (ZASP-PDZ bound to Act-EF1234). The coordinates of the RXCANDID bundle have been deposited in the PDB data bank (accession code 1rgw).